Article:
Poyraz, O., Tomlinson, D., Molyneux, A. et al. (2025) Optimized and additively manufactured face mills for enhanced cutting performance. Metals, 15 (4). 376. ISSN: 2075-4701

https://doi.org/10.3390/met15040376

metals

MDPI

Article

Optimized and Additively Manufactured Face Mills for Enhanced Cutting Performance

Ozgur Poyraz, Daniel Tomlinson, Anthony Molyneux, Marie E. Baxter, Evren Yasa * and James Hughes

The University of Sheffield Advanced Manufacturing Research Centre North-West, Blackburn BB2 7HP, UK; o.poyraz@amrc.co.uk (O.P.); d.tomlinson@amrc.co.uk (D.T.); a.molyneux@amrc.co.uk (A.M.); m.baxter@amrc.co.uk (M.E.B.); j.hughes@amrc.co.uk (J.H.)

* Correspondence: e.yasa@amrc.co.uk or e.yasa@sheffield.ac.uk

Abstract: With the growing acceptance of additive manufacturing (AM) across various sectors, laser-based powder bed fusion (PBF-LB) has widely been utilized to create intricately shaped parts from a range of metals alloys. The factors contributing to this reception are limited not only to the achievable geometrical complexity but also enhanced product functionality. Prominent sectors such as aerospace, defense, and biomedical have begun to leverage PBF-LB for a wide range of applications; its use in other industries, such as cutting tool manufacturing, remains more limited. Therefore, to address the potential of LPBF for higher performance in cutting tool applications, this study examines topology optimization and the laser powder bed fusion of face mills with experimental modal characteristics and cutting performance. The objectives in topology optimizations were to decrease the vibration magnitudes of face mills while keeping them stiff against deformation due to cutting forces. Three distinct designs were benchmarked, each with different weight reduction targets, and were fabricated using PBF-LB with M300 maraging steel. The optimized face mills demonstrated better performance with diminished vibration magnitudes and less tool wear patterns.

Keywords: laser-based powder bed fusion; maraging steel; topology optimization; face milling; tap testing; tool wear

Academic Editor: João Manuel R. S. Tavares

Received: 1 March 2025
Revised: 21 March 2025
Accepted: 25 March 2025
Published: 28 March 2025

Citation: Poyraz, O.; Tomlinson, D.; Molyneux, A.; Baxter, M.E.; Yasa, E.; Hughes, J. Optimized and Additively Manufactured Face Mills for Enhanced Cutting Performance. *Metals* **2025**, *15*, 376. https://doi.org/10.3390/met15040376

1. Introduction

Additive manufacturing (AM) has revolutionized product development, design, and manufacturing by enabling unprecedented geometrical freedom. Unlike traditional manufacturing methods, which often rely on fixtures, molds, or cores, AM builds objects layer by layer, offering the flexibility to design without the constraints imposed by conventional production techniques.

Along with its design and manufacturing advantages, AM offers a diverse range of material options, each suited to specific process categories. Today, a wide range of materials, including metals, polymers, ceramics, and composites are used in various AM technologies, to manufacture products enabling customized solutions across different industries. As per international standards organizations, AM technologies are categorized into seven distinct groups which include binder jetting (BJ), directed energy deposition (DED), material extrusion (ME), material jetting (MJ), powder bed fusion (PBF), sheet lamination (SL), and vat photopolymerization (VP) [1].

Among these techniques, laser-based powder bed fusion (PBF-LB), a subset of the PBF group, stands out as the most technologically mature method for processing metals and their alloys [2]. Currently, PBF-LB can process a diverse selection of metal alloys,

including aluminum, cobalt, copper, iron, nickel, and titanium alloys. Additionally, ongoing research is expanding to include materials previously unconsidered for PBF-LB, further enhancing the capabilities of the technique [3]. The process itself involves spreading a thin layer of fine metal powder over the build platform. This stage, influenced by different powder characteristics such as size, can impact process efficiency like spread ability and affect the part outcomes, including surface quality [4]. A laser, with a narrow focus and beam diameter of less than 100 µm, rapidly melts and solidifies the powder in the precise shape defined by the cross-section of the part. This layer-by-layer approach allows for the creation of complex geometries that would be challenging or even impossible to achieve using traditional manufacturing methods. With the combined application of a fine beam diameter and thin layer thicknesses, PBF-LB can create narrow melt pools to enable manufacturing of slender geometries [5], allowing the direct fabrication of intricate shapes such as turbine blades with internal cooling channels, impellers, or customized medical implants [6]. PBF-LB offers design flexibility through methods such as mass customization, topology optimization, lattice infilling for large volumes [7,8]. Industrial examples, such as the General Electric LEAP engine fuel nozzle, highlight the application of assembly consolidation, while topology optimization has been used to enhance the mechanical and dynamic properties of lightweight satellite structures [9,10].

Although the progress of topology optimization (TO) has been ongoing since 18th century with some considerable developments in theory and commercialization [11–14], it is the pairing of AM and TO that has shown to be an effective means for structural innovation, paving the path for broader applications [15]. As of today, density-based, hard-kill, boundary variation, and non-gradient topology optimization options are available under various commercial software packages, including Abaqus, Autodesk Fusion 360, Altair OptiStruct, Ansys Mechanical, Inspire, nTopology, and CAESS ProTOp [16]. Besides these, certain optimization software provides advanced features such as employing multiple objectives, integrating symmetrical solutions for effective computation, or executing calculations while taking various manufacturing constraints into account. Leveraging advancements in AM and TO, various industries such as aerospace, medicine, automotive industry, and machinery have launched numerous products, including gearboxes, engine brackets, landing gears, space frames, antenna enclosures, brake caliper casings, flywheels, and cam supports since the 2010s [16]. In contrast, the cutting tool sector has only begun its research and implementation efforts regarding the AM and TO of cutting tools and holders in recent years, mainly in the commercial domain.

Although metal tooling represents just 4% of total AM applications, a comprehensive literature review by Kelliger et al. (2024) revealed several possible advantages for cutting tools, categorized into cooling, light-weighting, damping, and functional integration through consolidation and topology optimization [17]. Figure 1 illustrates the categories of cutting tool materials and the potential enhancements achievable through the use of AM and TO [17].

Cutting tool cooling efficiency, which influences heat in the cutting zone, workpiece and tool temperatures, chip removal, and surface finish, can be significantly enhanced through AM. Lakner et al. (2019) demonstrated that an L-shaped nozzle design reduced flank wear when machining an AISI 4140 alloy [18]. Kugaevskii et al. (2019) further highlighted the effectiveness of AM in creating intricate shapes and efficient cooling holes [19]. Zäh et al. (2018) showcased the incorporation of spiral channels to improve cooling efficiency, made possible by the design flexibility of AM [20].

While vibration damping through lattice structures is a prevalent area of study, integrating these structures into cutting tools and minimizing the vibration amplitudes of the tools was only realized in 2019 by Vogel et al. [21]. They reengineered and produced a tool

holder featuring an elliptical cavity filled with truncated octahedron lattices, and tap tests indicated a reduction in amplitudes from 2.75 to 0.75 µm/N [21]. In a second investigation, they created a milling holder designed to include truncated octahedron elements filled alongside denser $WCZrO_2$ particles and demonstrated the findings through tap tests and acoustic emissions throughout milling [22]. Hanzl et al. focused on face mills where a cutter was restructured into a shell filled with body-centered cubic (BCC) lattice structures and subsequently tap tested to demonstrate its damping enhancement [23,24]. In research conducted by Tomasoni et al. (2021), a face mill underwent topological optimization, and the enhanced conditions related to displacement and stresses were reported [25].

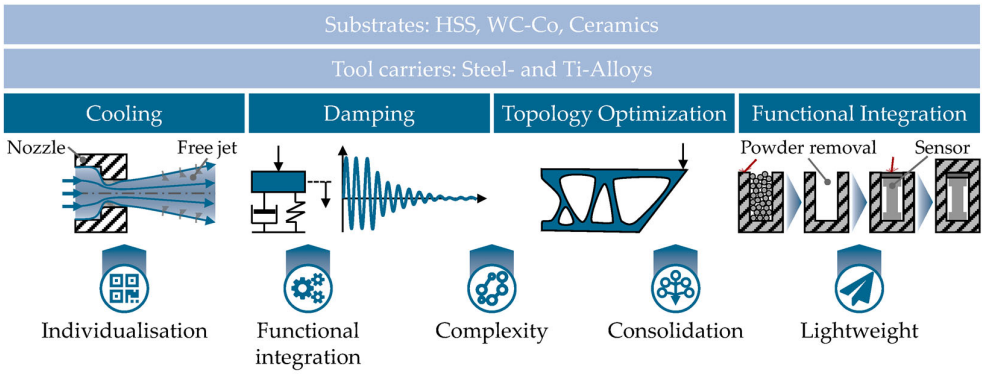

Figure 1. Potential cutting tool improvements via use of AM and TO by Kelliger et al. (licensed under CC BY 4.0) [17].

In addition to limited studies in academia, industrial cases have begun to emerge that leverage AM and integrate it with TO. These examples are provided by reputable tooling firms such as Kennametal, Sandvik Cormorant, and Seco. Kennametal's KENionic™ Technology provides lightweight poly-crystalline diamond (PCD) fine boring tools (Figure 2a), while Sandvik Coromant's Coromill lightweight Ti6Al4V face mill featuring silent mass-damped adaptors is sold commercially as an off-the-shelf product (Figure 2b). Furthermore, Seco Tools engages in hybrid AM tool production by building directly onto a HSK100 spindle cone (Figure 2c). Although industrial initiatives and advancements enhance the cutting-edge nature of AM tool design and production, access to detailed information from these case studies is limited due to IP considerations.

(**a**) (**b**) (**c**)

Figure 2. (**a**) Kennametal Lightweight PCD fine boring tool with steel body made with new KENionic ™ Technology (reprinted with permission from reference [26]); (**b**) Sandvik Coromill Light AM Tool with silent mass-damped adaptor (reprinted with permission from reference [27]); (**c**) Seco Hybrid AM tool for HSK interface (reprinted with permission from reference [28].

This article investigates the topology optimization of indexable face mills, considering modal characteristics into account as well as manufacturing constraints such as

overhangs. Face mills, additively manufactured from M300 maraging steel via PBF-LB, were machined to final dimensions and underwent tap tests and cutting trials on Ti6Al4V wrought plates. Outcomes were benchmarked based on insert wear patterns following one hour of machining.

2. Materials and Methods

This study follows the research outline in Figure 3, starting with the selection of a commercially available indexable face mill, followed by preliminary finite element analysis (FEA) to assess the tool's initial state. After topology optimizations based on initial FEA, distinct tool designs were produced from M300 maraging steel powder by PBF-LB AM and heat treated in accordance with the material's specification. Wire electric discharge machining (WEDM) was then used to separate the face mills from the PBF-LB base plates, and their assembly surfaces, such as the screw holes or insert seatings, were finish machined. The face mills were then mounted to spindle extension arbors and adaptors for tap tests. Lastly, cutting trials on wrought Ti6Al4V were carried out using a fixed set of cutting parameters.

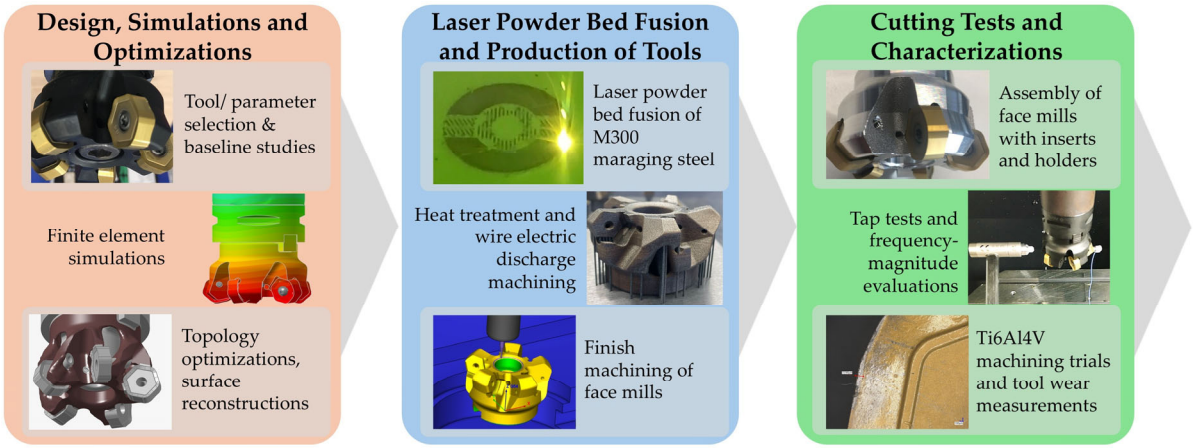

Figure 3. The research workflow for this study.

2.1. Design, Simulations and Optimizations

As a demonstrator, a 50 mm diameter indexable face mill with 5 cutting flutes suitable for cutting medium-to-high-strength materials was selected. The Kennametal Dodeka™ 45° (Spain) indexable face mill was used with a compatible KCSM40 carbide-grade insert with the serial number HNGJ 0905-ANSNGD (United States of America). The Sandvik HSK-to-Coromant Capto® adaptor (C5-390.410-63 090C) (Germany) and the Coromant Capto®-to-arbor adaptor (C5-391.05C-22 025M) were included in the tool holding assembly, which was maintained at 115 mm length as an intermediate value (Figure 4a). Antivibration boring bars were intentionally omitted from the study.

FEA and TO were conducted with Altair Inspire© 2023.1 which invokes OptiStruct© 2023.1 for solving. Solid 3-dimensional (Tetra10/CTETRA) mesh elements were used for both the preliminary FEA and the latter TO. The reason for this preference is the ability of these elements to adapt to intricate geometric forms. Variable mesh sizes were used, and the ratio of meshes with a skew (distortion) of 0.999 was targeted to be below 0.1% for the whole assembly to maintain high quality.

Spindle extension, arbor, and inserts were chosen as non-design areas for optimizations, indicating that they cannot undergo any material removal or weight reduction (Figure 4a). Even though the face mill body was viewed as a design area, the mating

features were divided and excluded from optimizations to maintain the assembly integrity (Figure 4d).

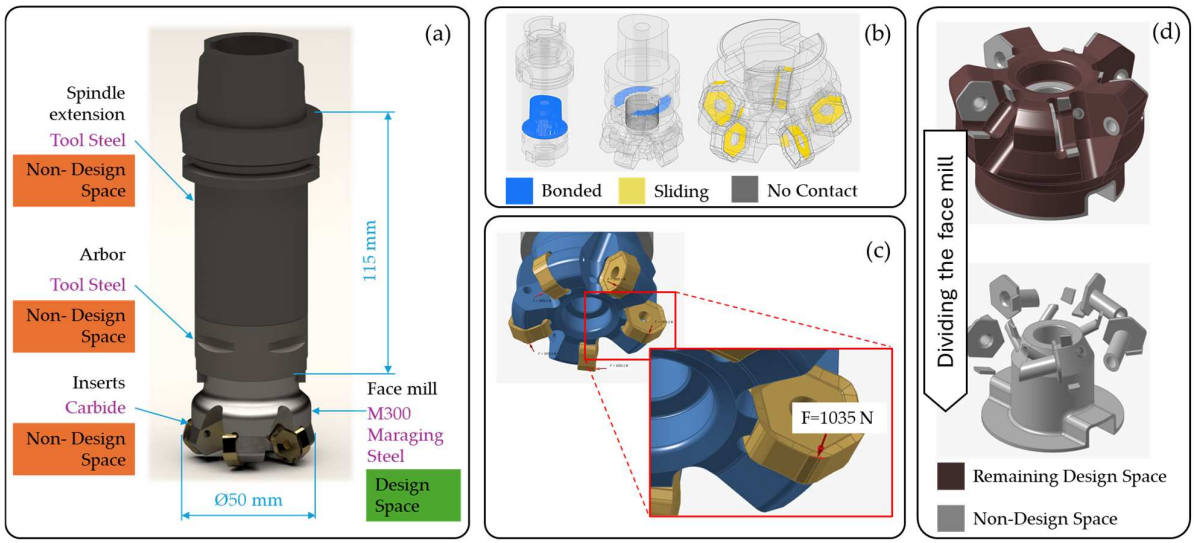

Figure 4. (**a**) Face mill assembly with component names, dimensions and materials, (**b**) contacts, (**c**) force boundary conditions, (**d**) design and non-design spaces of face mill body.

It was assumed that the contact between the inserts and the face mill was frictionless linear sliding. Bonded contacts were assigned between the remaining bodies, excluding the cylindrical face of the arbor that extends into the face mill in a loose state (Figure 4b).

To supply cutting forces as boundary conditions for FEA and TO, computer-aided manufacturing (CAM) and cutting force simulations were conducted. Toolpaths were created in Siemens NX 2412, utilizing a linear zig strategy to ensure climb cutting was maintained. For the FEA and TO, higher cutting parameters were considered to ensure safety and prevent the damage or deformation of the optimized face mills during testing. In this context, 50 m/min cutting speed (V_c), 0.31 mm feed per tooth (f_z), 2.25 mm axial depth of cut (a_p), and 30 mm radial depth of cut (a_e) were chosen. Cutting force simulations were performed with MACHPRO™ software, utilizing cutting force coefficients previously obtained by AMRC NW researchers, revealing a maximum force value of 1035 N in the tangential direction, which was used as a boundary condition for FEA and TO (Figure 4c).

A fixed constraint was applied to the spindle and machine interface, and 80% pretension loads were considered for the fasteners, including the inserts and the arbor.

The main goal for TO was to achieve weight reductions of at least 15%, 25%, and 35%, aiming to enhance the modal condition of the face mills by increasing frequencies or decreasing vibration magnitudes. Since reducing the weight and volume/thickness of the components could negatively affect the stiffness, the increases in deformation relative to the original face mill were also restricted to 20%, 25%, and 30%. Finally, rotational symmetry was incorporated into TO, and a manufacturing constraint of an overhang angle of 45° was implemented to facilitate support-free PBF-LB. The material properties used for FEA and TO are presented in Table 1 along with their corresponding references.

Table 1. Material properties used for FEA and TO.

Material	Density (kg/m^3)	Elastic Modulus (GPa)	Yield Strength (MPa)	Reference No.
M300	8100	199	1873	[29]
Tool Steel	7800	210	1650	[30]
Carbide	15,700	669	300	[31]

As the TO process reduces weight by discarding or voiding the mesh elements that are not necessary according to the analysis, faceted geometries and volumes were created. Due to the faceted shapes, these rough volumes need to be reconstructed to be utilized for subsequent operations. The majority of the surface reconstruction steps were performed using the Siemens NX 2412 Polygon Modeling module, incorporating the other components of assembly like the arbor and inserts. Additionally, the PolyNURBS Modeling module of Altair Inspire© 2023.1 was used for certain freeform surfaces that necessitated more complex forms and transitions. The final modifications on face mill designs were carried out by following Design for Additive Manufacturing (DfAM) principles. In this regard, the rotational axes of the face mills were adjusted to be parallel to the PBF-LB build direction, and their arbor mating faces were kept at the bottom, as these assembly faces would eventually require finish machining. Face mill geometries were then subjected to draft angle analysis based on a 45° overhanging limit, leading to a lower volume of supports. This achievement is also related to the overhang control constraint that was introduced for TO. As the last step, 0.5 mm stock envelopes were added to the up-facing mating surfaces like screw holes, insert seats and arbor interfaces.

2.2. Laser Powder Bed Fusion and Production of Face Mills

Carpenter Additive® gas atomized M300 maraging steel (United Kingdom) powders were employed for PBF-LB. M300 powder having iron as the balancing element contains the primary alloying elements of nickel at 18.2% weight, cobalt at 9.0% weight, molybdenum at 4.85% weight, and titanium at 0.87% weight. The M300 maraging steel used for this project exhibited an average powder size distribution of 35 µm with Dv (10) 19 µm and Dv (90) 52 µm levels.

PBF-LB production was conducted using a Renishaw® AM250 (United Kingdom) system located at the Royce Translational Centre (RTC) at the University of Sheffield. To ensure the reliability and repeatability of the additive manufacturing process, the machine underwent a comprehensive optical calibration and verification performed by the OEM. Routine servicing is conducted, including a thorough inspection to confirm optimal performance. This system features a 250 × 250 mm build area, a pulsed ytterbium fiber laser and an argon as an inert gas atmosphere. Volumes of both unoptimized and optimized face mill geometries were exported to a standard tessellation language (stl) file format, sliced with Materialise® Magics version 28, and prepared using Renishaw QuantAM software version 5.3. Pyramid type support structures were used where necessary, and density cubes were also included to validate the density of parts (Figure 5a).

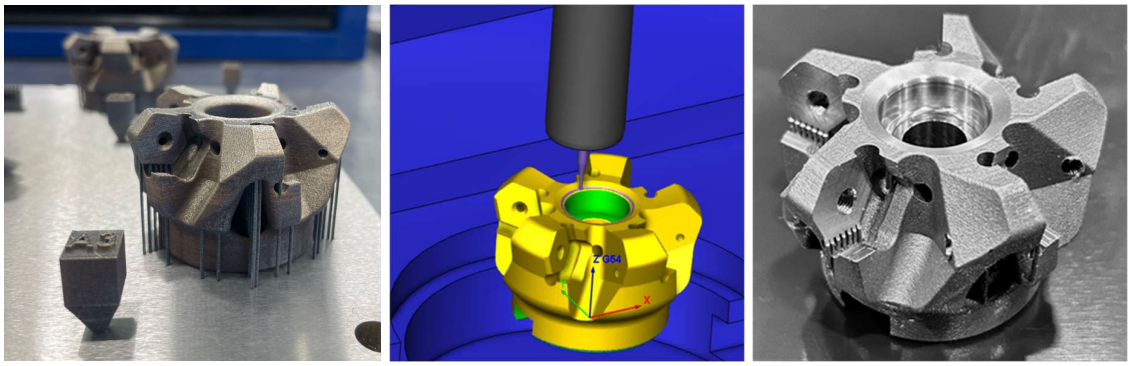

(**a**) (**b**) (**c**)

Figure 5. (**a**) Face mill and density cube and support structures following LPBF, (**b**) machining simulation using Vericut, (**c**) finished face mill.

The bulk material, or hatch region, was processed using a laser power of 200 W, a point distance of 65 µm, and an exposure time of 80 µs, with a hatch distance of 80 µm. The border was processed with a reduced laser power of 100 W, a finer point distance of 20 µm, and an exposure time of 50 µs to refine edge quality and minimize surface roughness. Both scanning strategies resulted in an equivalent scanning speed of 528 mm/s. The layer thickness was maintained at 40 µm to ensure a balance between build rate and part density.

The parts were heat treated in a TAV vacuum furnace (Model TH 30/30/30). The heat treatment recipe that was carried out on the samples is the standard stress-relief (SR) cycle recommended by the machine manufacturer [32]. The ramp up rate from room temperature was 10 °C per minute up to 850 °C, at which temperature the dwell time was 30 min, followed by an argon air cool. Following the SR, the parts were separated from the base plate using a GF AgieCharmilles CUT 550 P (Switzerland) wire electric discharge machine (WEDM).

Density measurements following Archimedes' principle were performed in accordance with ASTM 962-23 on a precision balance (Precisa Series 360 EP 125 SM) using distilled water. The results confirmed densities exceeding 99.9% [33].

The computer-aided manufacturing (CAM) for the face mills was conducted with Siemens NX 2412, and once the toolpaths were post-processed and transformed into G-codes, CGTech VERICUT 9.5.1 was employed for simulations to prevent any collisions on the machine. Finally, stock envelopes of 0.5 mm were finish machined on a Hermle C400 multi-axis milling machine located at AMRC NW (Figure 5b,c).

2.3. Tests and Investigations

Quality control of the produced tools was performed with respect to dimensional and surface quality factors. They underwent 3-dimensional (3D) scanning with the GOM ATOS-Q scanner, and stl models were generated using GOM Inspection software version 2021. Subsequently, these models were brought into Siemens NX 2412 along with nominal CAD files, and the software's automatic fitting option was utilized to best fit these two models. A 3D deviation gauge was utilized for a checking distance of 0.250 mm and an inner and outer tolerance of 0.02 mm. Surface quality inspections were conducted on specific surfaces of each produced face mill. These critical surfaces include the flat plane between the face mill and arbor, the insert seatings, the tips, and the radial outer diameter. These were measured using a Keyence VHX E-100 microscope (Japan) at 500× magnification. After taking measurements, VHX software was employed in 3D depth mode to obtain surface quality values. The arithmetic mean of the surface areas (Sa) was chosen to compare various face mills by setting the S-Filter to 2.5 µm and the L-Filter to 4 µm. After dimensional and surface quality assessments, each face mill was weighed using a Kern KB10000-1N balance, which has a readability increment of 0.1 mm.

As an assembly inspection, all face mills were assembled with spindle extensions, arbors, and inserts. Certain mating conditions, such as insert to face mill, were evaluated with a height gage and shims to identify any problems concerning their alignment or gaps between them. Additionally, the radial and axial runouts of insert tips were measured using a Nikken Elbo Controlli E46LA Tool Presetter and compared to those fitted on the original equipment manufacturer (OEM) face mill.

Final tap tests were carried out on the Mazak Variaxis I500 (Japan) utilizing the Productive Machines TapStarter kit (United Kingdom). This was utilized with the ICP 50,862 hammer, PCB Model 352C23 accelerometer, and the ICP Model 485B39 sensor signal conditioner, all of which were properly calibrated. Tap testing began solely with spindle extension, followed by the sequential addition of arbor, OEM face mill, and inserts (Figure 6a). This procedure was also carried out for additively manufactured face mills

considering two axial directions as X and Y. The outputs were received as csv files in a columnar format, including frequency (1–10,000 Hz) and magnitude (m/N). In creating the frequency and magnitude graphs for this article, the resulting real and imaginary values were considered, and the averages of the X and Y directions are presented to provide a summary of numerous measurements. The frequency range of 300–1300 Hz was plotted to prevent any negligible values, emphasize the key window, and clearly present the benchmark within the focused range.

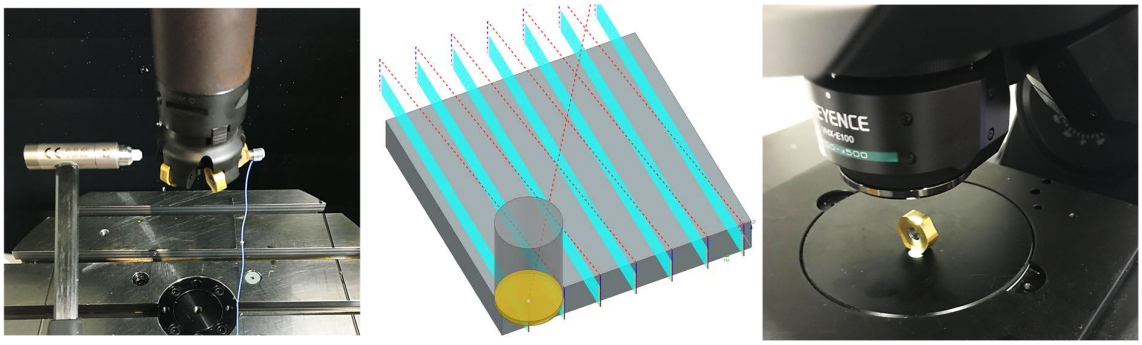

(**a**) (**b**) (**c**)

Figure 6. (**a**) Tap testing of face mills, (**b**) zig cutting strategy for machining tests, and (**c**) flank wear measurements under microscope.

Machining tests were performed on a Mazak Variaxis I500, located at AMRC NW, using four plates of Ti6Al4V (ASTM Grade 5 titanium) alloy with dimensions of 200 × 200 × 50 mm^3 [34]. A zig cutting strategy was employed to keep each parameter and climb cutting the same throughout all machining (Figure 6b); 60 m/min cutting speed (Vc), 0.113 mm feed per tooth (fz), 2 mm axial depth of cut (ap), and 30 mm radial depth of cut (ae) were considered, and toolpath generation was accomplished using Siemens NX CAM module. Tests were deliberately paused at the 30 min mark during the cutting process to assess the progress of the tool wear and finished after 1 h of cutting.

International standards define tool deterioration as the changes observed on the cutting edge of tools resulting from the process of cutting [35]. Although this is a broad term, the standards encompass tool wear and brittle fractures or chipping as subcategories of deterioration. Among them, tool wear or flank wear refers to the loss of tool material from the flanks of the tool during the cutting process and it can be uniform (VB1), non-uniform (VB2), or localized (VB3) at certain locations. The standard suggests limits of 0.3 mm for uniform (VB1) wear and 0.5 mm for localized (VB3) wear [35]. Alongside the standards, earlier research on tool wear during Ti6Al4V machining has performed wear tests over specific time periods. In this context, prior researchers performed wear tests based on a 0.3 mm uniform tool wear limit, which lasted from thirty minutes to one hour [36,37]. Considering these factors, flank wear studies were conducted, and the flanks of 5 inserts from each face mill were examined using a Keyence VHX E-100 microscope at 100× magnification (Figure 6c). Inserts were positioned under the microscope at a right angle to the lens to observe the flank faces, and measurements were obtained using the length measurement feature of VHX Software.

Finally, the surface quality of the machined plates was measured along feed and cross-feed directions. The portable Mitutoyo Surftest SJ-210-Series 178 (Japan) was employed for roughness assessments utilizing constant sampling lengths and cut-off lengths (λs = 2.5 μm, λc = 0.8 μm) for each machined plate. The arithmetic mean values (Ra) were reported as the outcomes.

3. Results and Discussions

The preliminary FEA outcomes offered an in-depth understanding of the OEM tool's modal characteristics and deformation behavior under the stresses induced by cutting forces. The initial modal analysis of the tool assembly, consisting of the OEM face mill and inserts, revealed bending in various X and Y directions in the first modes, followed by torsional motion around the tool's rotational center, and culminating in axial displacement in the sixth mode. The results of the FEA simulations confirmed that the OEM face mill is already a stiffness-driven component, and it did not appear to be susceptible to high deformations under the applied loading conditions. Even under the worst-case scenario—where a cutting force of 1035 N is applied due to the previously outlined aggressive cutting parameters—the maximum elastic deformation the OEM tool experiences was observed at approximately 52 µm.

Since some of the TO gave way to an irregular and inhomogeneous mesh distribution near insert mating faces, surface reconstructions needed careful consideration. There were detached regions close to the insert mating faces in just one of the results, Option 3, which had the most ambitious mass reduction target. The Polygon Modeling module of Siemens NX 2412 and the PolyNURBS modeling module of Altair Inspire were used to overcome these problems; however, this revealed the necessity of FEA simulations on the new geometries. Figure 7 shows the results of FEA simulations of the reconstructed face mills that were optimized by aiming for minimum mass reductions of 15%, 25%, and 35%, respectively, for the three options. These optimizations also limited the deformation increase relative to the OEM face mill to less than 20%, 25%, and 30%. As can be seen in Figure 7, all optimization targets regarding the mass reduction were successfully met and none of the deformation constraints were violated.

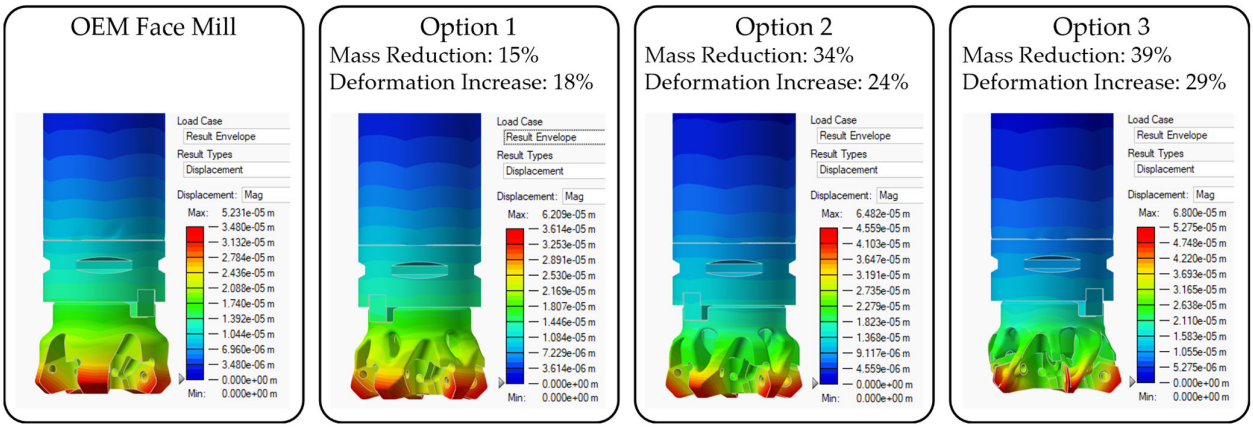

Figure 7. Benchmarking of TO results in terms of mass reduction and deformation increase.

The highest deformation increase ratio of 29%, which changed the OEM tool's 52.3 µm deformation to 68 µm for TO Option 3, still remained within elastic limits. This conclusion was confirmed by examining the stress graphs produced by FEA simulations (see Figure 8). The graph illustrates the von Mises stress levels of the tool bodies, accompanied by a common color legend on the right side. The highest stress observed in those limited areas for various TO options reached approximately 450 MPa, providing a sufficient buffer from the yield stress and preventing the risk of plastic deformations.

The reconstructed face mill geometries were produced via PBF-LB, SR and machining without any significant problems. The 3D scans of the produced face mills exhibited good dimensional accuracy in comparison to the nominal CAD model and all adhered to the tolerances specified in the Materials and Methods section. The surfaces of unoptimized AM face mills showed Sa values ranging from 0.7 µm to 1.5 µm, since they were generally

machined post PBF-LB, whereas optimized face mills could only achieve this range for the flat plane between the face mill and arbor, as well as the insert seatings. The remaining freeform surfaces of all optimized face mills, particularly in the outer radial regions, showed a rougher nature, reaching Sa 14.28 µm due to the well-known stair stepping effect.

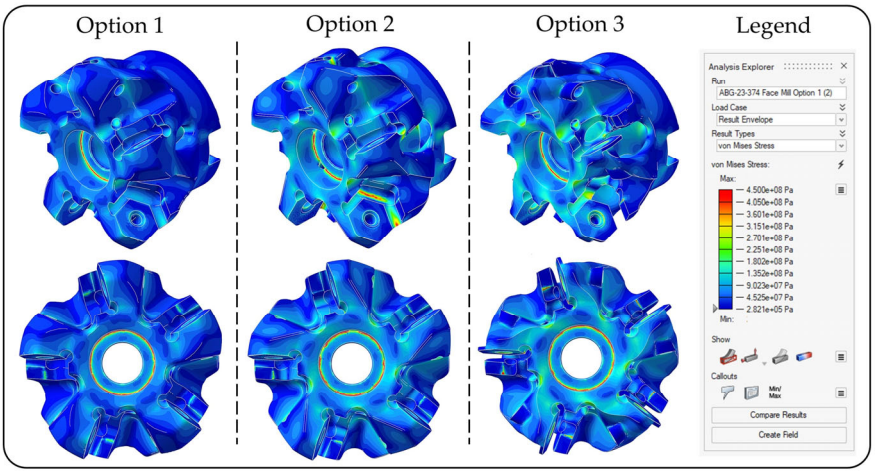

Figure 8. Benchmarking of TO results in terms of von Mises stresses.

The weight of the tools also differed due to the variations in geometries resulting from TO. As can be seen in Table 2, every optimized face mill exhibited a reduced mass when compared to the original face mill. Conversely, only the unoptimized AM face mill was heavier than the original face mill. This is because, while the volumes of both options are identical, the density of M300 maraging steel (8.1 g/cm^3) surpasses the density of the original face mill material (7.8 g/cm^3), AMS 6411 [29,38].

Table 2. Comparison of face mill masses.

	Original Face Mill	Unoptimized AM Face Mill	TO Option 1 Face Mill	TO Option 2 Face Mill	TO Option 3 Face Mill
Mass (g)	329	344	279	213	201

In addition to Figures 7 and 8, which illustrate deformations and stresses, Figure 9 compares the modal characteristics based on tap test results. Figure 9a demonstrates that tap testing solely on the extension body produced a distinct peak at approximately 1100 Hz, which was identified as the dominant frequency associated with the extension body. Upon the installation of the arbor on the extension, a new peak emerged at approximately 700 Hz, and the dominant frequency of the extension body was shifted to 1000 Hz with a significant increase in its magnitude (Figure 9b). Finally, addition of OEM face mill and inserts introduced a new peak around 500 Hz, while shifting the extension's dominant frequency to 900 Hz and increasing the magnitude of extension and arbor to around 700 Hz (Figure 9c). When the results from the OEM face mill were compared with TO Option 3, a distinct advantage of weight reduction in vibration magnitude was apparent in the 400–500 Hz frequency range (Figure 9d). After observing the advantages from the comparison of the OEM face mill and TO Option 3, the other TO options (Option 1, Option 2) and an additively manufactured version of the OEM face mill geometry were also evaluated within the same frequency range. While TO Option 1 and TO Option 2 showed benefits compared to the tool assembly with the OEM face mill, their ability to reduce vibration magnitude was less effective than that of Option 3. The unoptimized additively manufactured face mill assembly exhibited higher vibration levels than the OEM face mill assembly. This outcome

was associated with the higher mass of unoptimized AM face mill when compared to the mass of the original face mill (Table 2).

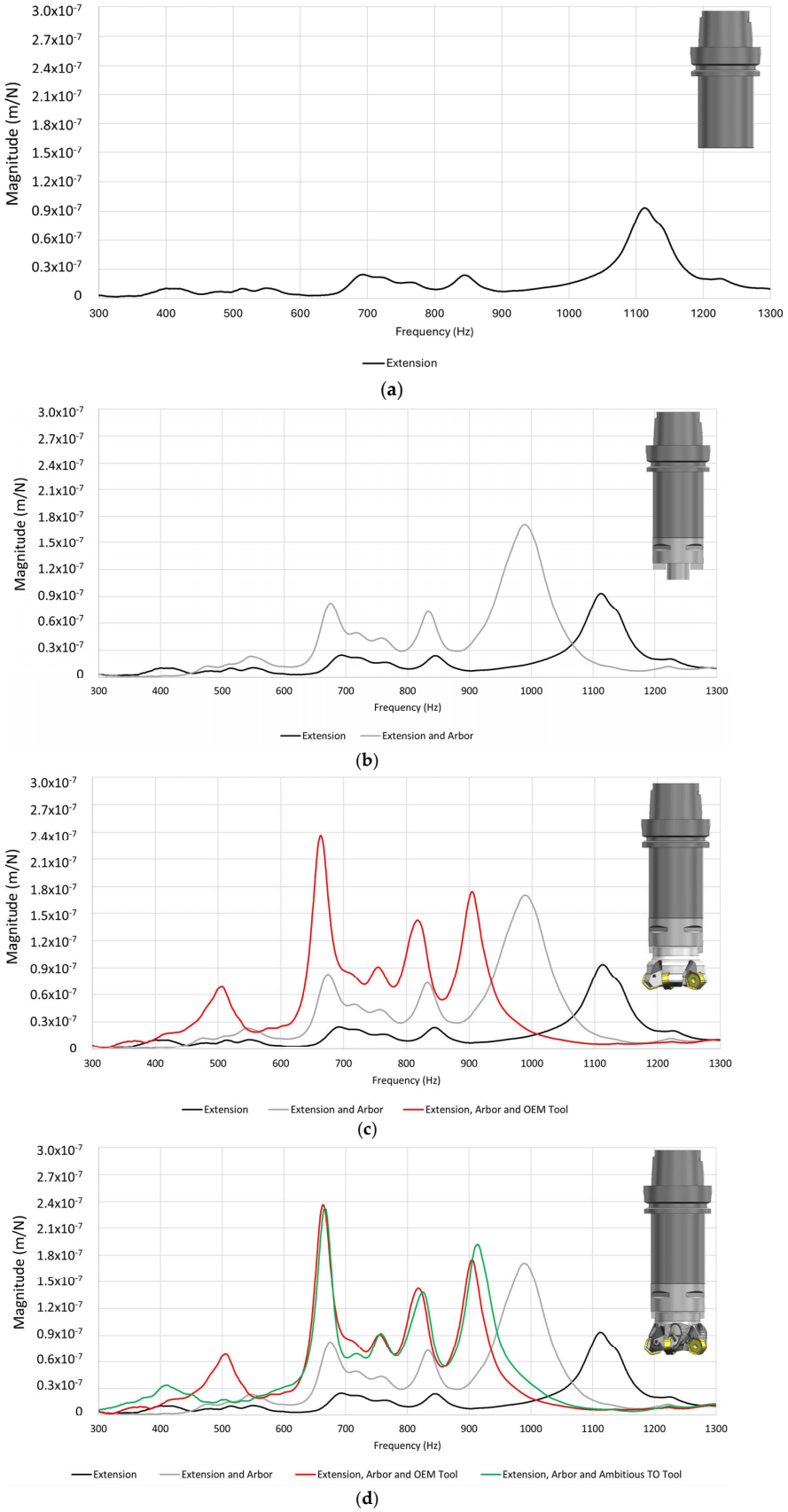

Figure 9. Tap testing results: (**a**) extension; (**b**) extension and arbor; (**c**) extension arbor and OEM tool; (**d**) extension, arbor, and OEM tool benchmarked with extension, arbor, and TO Option 3.

It was observed that all tools could operate for about 1 h on one cutting edge before hitting the average flank wear (VB1) limit of 0.3 mm, as shown in Figure 10, as recommended by the standard [35]. Considering the six edges on each insert and both sides, these tools could potentially be effective for up to 12 h. Since the distances of the localized flank wear (VB3) peaks to the insert tip were 2 mm in most instances, this suggests a correlation with a 2 mm cutting depth, allowing for the interpretation of notch wear (Figure 11). Nonetheless, it is acknowledged that stability problems during the cut may exacerbate notch wear.

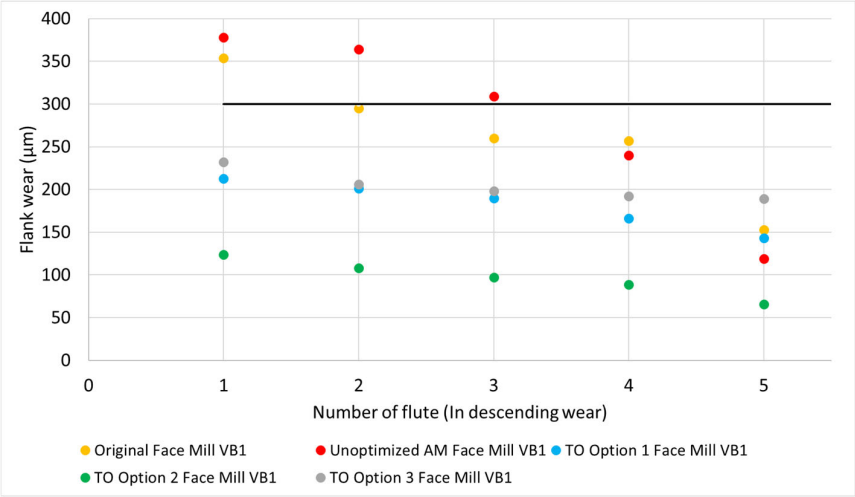

Figure 10. Average flank wear of various face mills listed according to the number of flutes in decreasing order of wear.

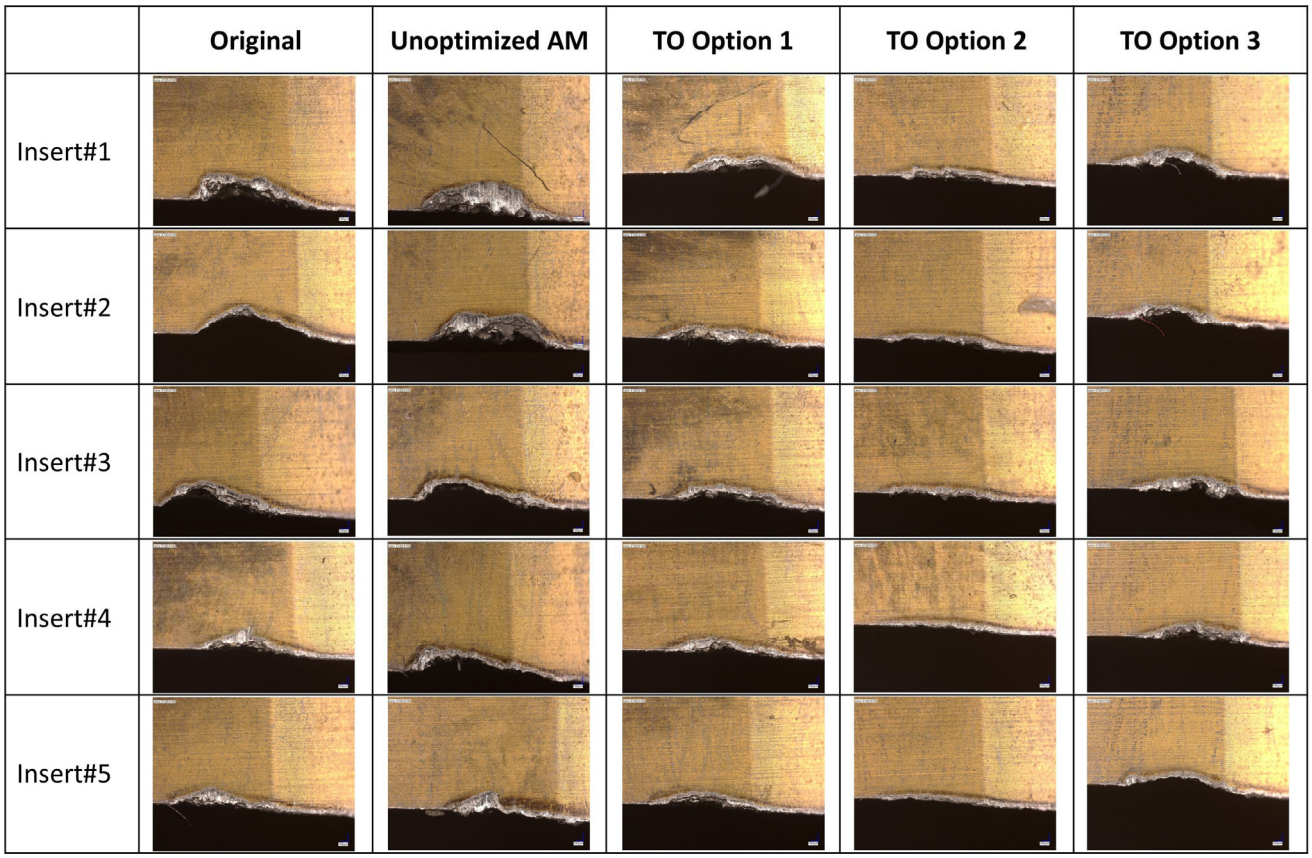

Figure 11. Benchmarking of worn edges of various face mill inserts.

The optimal outcomes were seen with TO Option 2, which had a moderate mass reduction, whereas the least favorable results were linked to the unoptimized AM tool. Of the three optimized versions, the TO Option 3 face mill had the lowest performance. Despite having more ambitious optimization goals than the other two, which results in greater reductions in mass and vibration magnitude, this observation might be linked to micro deflections in thin insert supports during the process, causing variations in chip thickness. On the other hand, the thinner sections may be less effective than the thicker ones at transferring heat to the arbor and extension body, resulting in the reduced cooling of the face mill and inserts. However, in this study, the effect of the coolant was not taken into consideration, and it is possible that this optimized geometry might have led to some unfavorable conditions regarding the cooling. Figure 11 illustrates that the inserts from TO Option 1, TO Option 2, and TO Option 3 face mills with reduced wear showed minimal variation among themselves, and the average flank wear across various inserts stayed within a steady range. The variations in average flank wear among different inserts of the original face mill and the unoptimized AM face mill ranged from 0.15 m to 0.35 mm.

Ti6Al4V plates that were machined and benchmarked with the original face mill and the topologically optimized AM face mills exhibited the same surface roughness values of Ra 0.3 µm in the cross-feed direction. On the other side, the surface roughness measurements in the feed direction fluctuated within a small range, with the original face mill demonstrating Ra 0.29 µm, whereas the optimized face mills exhibited an average of Ra 0.21 µm.

The economic viability of employing additive manufacturing technologies for producing face mills was examined once all technical evaluations were finished. Although the real cycle time computations were executed for all AM face mills taking into account PBF-LB, SR, and machining phases, an estimation was made for the conventional face mill by programming creep feed grinding of the flutes using parameters outlined in the article by Dang et al. (2022) [39]. These cycle times were subsequently multiplied by staff costs and machine charge rates. Ultimately, the costs for materials and tools were combined to determine the overall price. Since the information concerning costs is commercially confidential, the results were normalized as a percentage and are shown in Figure 12. As shown in Figure 12, the unoptimized AM face mill is the priciest tool due to its lengthy PBF-LB step, along with significant costs resulting from machining and powder material usage. Contrary to this, the original face mill, utilizing a conventional machining method that includes grinding, turning, and milling, exhibits the least production expenses. It is essential to emphasize that the material costs of the original face mill are this low and cannot be observed in the graph. Of the optimized variants, just TO Option 3 face mill can come close to the reduced expenses of original face mill, yet continues to exhibit elevated figures.

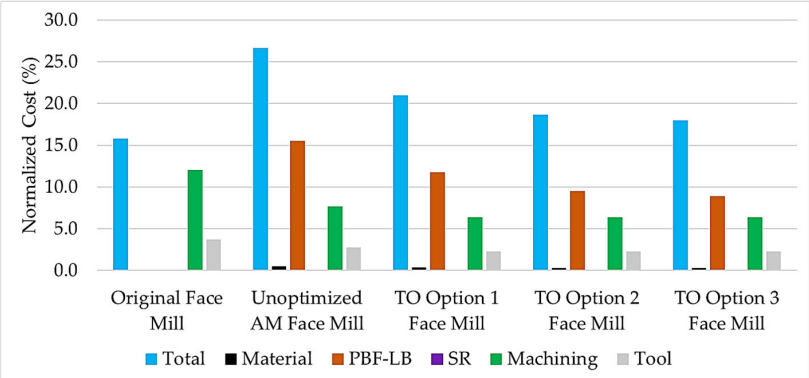

Figure 12. Normalized costs of tool productions.

4. Conclusions

This research demonstrated the application of topology optimizations and additive manufacturing of indexable face mills to improve cutting efficiency. Three weight reductions were evaluated to lower the vibration magnitudes of tool assemblies while maintaining deformation similar to traditional counterparts and within elastic limits. By outlining all essential procedures, such as surface reconstruction, laser powder bed fusion, heat treatment, and machining, it was shown that various objectives can be accomplished through the application of the suggested methodology and workflow. The advantages of utilizing optimized tools highlighted an extension of the insert tool life and successfully reduced flank wear to 100 µm after one hour of machining Ti6Al4V.

Author Contributions: Conceptualization, E.Y. and O.P.; methodology, O.P., D.T., M.E.B., A.M. and E.Y.; validation, D.T., A.M. and M.E.B., investigation, D.T., A.M., M.E.B. and O.P.; writing—original draft preparation, O.P. and E.Y.; writing—review and editing, E.Y. and J.H.; supervision, E.Y. and O.P.; project administration, J.H. and E.Y.; funding acquisition, J.H. and E.Y. All authors have read and agreed to the published version of the manuscript.

Funding: This research was funded by AMRC Membership Funding under ABG-23-374 Project entitled as "Additively Manufactured Face Mill Development FoR EnhancEd Machining (FREE)".

Data Availability Statement: The original contributions presented in this study are included in the article. Further inquiries can be directed to the corresponding author.

Acknowledgments: The authors of the study would like to acknowledge Abdul Haque for initial LPBF layout preparation and M. Bora Islier for project management related activities. Kennametal's approval to utilize their face mill as a benchmark is very much appreciated, along with Andy Boffin's and Werner Penkert's technical support and rigorous review of project tasks. Finally, the authors express their gratitude to Kennametal, Sandvik and Seco Tools for providing the images of their advanced additively manufactured face mills.

Conflicts of Interest: The authors declare no conflicts of interest.

Abbreviations

The following abbreviations are used in this manuscript:

3D	Three-dimensional
AM	Additive manufacturing
BCC	Body centered cubic
BJ	Binder jetting
CAM	Computer aided manufacturing
DED	Directed energy deposition
DfAM	Design for additive manufacturing
Dv (X)	Particle size distribution for X percentage
FEA	Finite element analysis
ME	Material extrusion
MJ	Material jetting
OEM	Original equipment manufacture
PBF	Powder bed fusion
PBF-LB	Laser-based powder bed fusion
PCD	Ploy crystalline diamond
SR	Stress relieved
stl	Standard tessellation language file format
TO	Topology optimization

VB	Flank wear
Vc	Cutting speed
WEDM	Wire electric discharge machining

References

1. Martínez-García, A.; Monzón, M.; Paz, R. Standards for Additive Manufacturing Technologies. In *Additive Manufacturing*; Elsevier: Amsterdam, The Netherlands, 2021; pp. 395–408, ISBN 9780128184110.
2. Leary, M.; Downing, D.; Lozanovski, B.; Harris, J. Design Principles. In *Fundamentals of Laser Powder Bed Fusion of Metals*; Elsevier: Amsterdam, The Netherlands, 2021; pp. 119–154, ISBN 9780128240908.
3. Guan, J.; Wang, Q. Laser Powder Bed Fusion of Dissimilar Metal Materials: A Review. *Materials* **2023**, *16*, 2757. [CrossRef] [PubMed]
4. Lupo, M.; Ajabshir, S.Z.; Sofia, D.; Barletta, D.; Poletto, M. Experimental Metrics of the Powder Layer Quality in the Selective Laser Sintering Process. *Powder Technol.* **2023**, *419*, 118346. [CrossRef]
5. Depboylu, F.N.; Yasa, E.; Poyraz, O.; Korkusuz, F. Thin-Walled Commercially Pure Titanium Structures: Laser Powder Bed Fusion Process Parameter Optimization. *Machines* **2023**, *11*, 272. [CrossRef]
6. Kundakcıoğlu, E.; Lazoglu, I.; Poyraz, Ö.; Yasa, E. Modeling of Residual Stress and Distortion in Direct Metal Laser Sintering Process: A Fast Prediction Approach. *Prod. Eng. Res. Dev.* **2022**, *16*, 769–783. [CrossRef]
7. Flores, I.; Kretzschmar, N.; Azman, A.H.; Chekurov, S.; Pedersen, D.B.; Chaudhuri, A. Implications of Lattice Structures on Economics and Productivity of Metal Powder Bed Fusion. *Addit. Manuf.* **2020**, *31*, 100947. [CrossRef]
8. Eren, O.; Kürşad Sezer, H.; Ersel Canyurt, O. Perspective Chapter: Design Considerations for Additive Manufacturing. In *Product Design—A Manufacturing Perspective*; Yasa, E., Poyraz, O., Eds.; IntechOpen: London, UK, 2024; ISBN 9781803565545.
9. Khorasani, M.; Ghasemi, A.; Rolfe, B.; Gibson, I. Additive Manufacturing a Powerful Tool for the Aerospace Industry. *Rapid Prototyp. J.* **2022**, *28*, 87–100. [CrossRef]
10. Hurtado-Pérez, A.B.; Pablo-Sotelo, A.D.J.; Ramírez-López, F.; Hernández-Gómez, J.J.; Mata-Rivera, M.F. On Topology Optimisation Methods and Additive Manufacture for Satellite Structures: A Review. *Aerospace* **2023**, *10*, 1025. [CrossRef]
11. Goldstine, H.H. *A History of the Calculus of Variations from the 17th Through the 19th Century*; Studies in the History of Mathematics and Physical Sciences; Springer: New York, NY, USA, 1980; Volume 5, ISBN 9781461381082.
12. Maxwell, J.C.I. On Reciprocal Figures, Frames, and Diagrams of Forces. *Trans. R. Soc. Edinb.* **1870**, *26*, 1–40. [CrossRef]
13. Bendsøe, M.P.; Kikuchi, N. Generating Optimal Topologies in Structural Design Using a Homogenization Method. *Comput. Methods Appl. Mech. Eng.* **1988**, *71*, 197–224. [CrossRef]
14. Altair. Topology Optimization and the Lessons of History. 2020. Available online: https://altair.com/blog/executive-insights/Topology-Optimization-and-the-Lessons-of-History#:~:text=As%20the%20world%20leader%20in,also%20saw%20the%20competitive%20advantages (accessed on 21 January 2025).
15. Liu, S.; Li, Q.; Hu, J.; Chen, W.; Zhang, Y.; Luo, Y.; Wang, Q. A Survey of Topology Optimization Methods Considering Manufacturable Structural Feature Constraints for Additive Manufacturing Structures. *Addit. Manuf. Front.* **2024**, *3*, 200143. [CrossRef]
16. Ibhadode, O.; Zhang, Z.; Sixt, J.; Nsiempba, K.M.; Orakwe, J.; Martinez-Marchese, A.; Ero, O.; Shahabad, S.I.; Bonakdar, A.; Toyserkani, E. Topology Optimization for Metal Additive Manufacturing: Current Trends, Challenges, and Future Outlook. *Virtual Phys. Prototyp.* **2023**, *18*, e2181192. [CrossRef]
17. Kelliger, T.; Meurer, M.; Bergs, T. Potentials of Additive Manufacturing for Cutting Tools: A Review of Scientific and Industrial Applications. *Metals* **2024**, *14*, 982. [CrossRef]
18. Lakner, T.; Bergs, T.; Döbbeler, B. Additively Manufactured Milling Tool with Focused Cutting Fluid Supply. *Procedia CIRP* **2019**, *81*, 464–469. [CrossRef]
19. Kugaevskii, S.; Pizhenkov, E.; Gamberg, A. The Effectiveness of Additive SLM-Technologies in the Manufacture of Cutting Tools. *Mater. Today Proc.* **2019**, *19*, 1977–1981. [CrossRef]
20. Zäh, M.; Seidel, C.; Sellmer, D. *Technologie Report 08—Additive Fertigung*; MAPAL Präzisionswerkzeuge Dr. Kress KG: Aalen, Germany, 2018.
21. Vogel, F.A.M.; Berger, S.; Özkaya, E.; Biermann, D. Vibration Suppression in Turning TiAl6V4 Using Additively Manufactured Tool Holders with Specially Structured, Particle Filled Hollow Elements. *Procedia Manuf.* **2019**, *40*, 32–37. [CrossRef]
22. Vogel, F.; Baumann, J.; Jaquet, S.; Biermann, D. Particle Damped Tool Holders Enable Higher Stability Limits When Milling EN AW-7075. *SSRN J.* **2023**, 77–84. [CrossRef]
23. Hanzl, P.; Zetek, M.; Rulc, V.; Purš, H.; Zetková, I. Finite Element Analysis of a Lightweight Milling Cutter for Metal Additive Manufacturing. *Manuf. Technol.* **2019**, *19*, 753–758. [CrossRef]
24. Hanzl, P.; Zetková, I.; Zetek, M. Comparison of Lightweight and Solid Milling Cutter Capabilities. *Manuf. Technol.* **2020**, *20*, 23–26. [CrossRef]

25. Tomasoni, D.; Giorleo, L.; Ceretti, E. Milling Tool Optimization by Topology Optimization Technique. *ESAFORM* **2021**, *2021*, 1–10. [CrossRef]
26. Kennametal. Kennametal Innovation Earns International Recognition as Recipient of R&D 100 Award. 2023. Available online: https://www.kennametal.com/de/en/news/123114.html (accessed on 23 January 2025).
27. Sandvik. How 3D-Printing and Titanium Became Game-Changers for Lightweight CoroMill® 390. 2020. Available online: https://www.metalpowder.sandvik/en/news-media/news/2020/07/additive-manufacturing-and-titanium-optimized-the-lightweight-coromill-390/ (accessed on 12 February 2025).
28. Seco. Seco Tools 3D Manufacturing Creates New Opportunities. 2023. Available online: https://www.secotools.com/article/123840?language=en (accessed on 12 February 2025).
29. Renishaw. M300 Maraging Steel Data Sheet. 2017. Available online: https://www.renishaw.com/resourcecentre/download/datasheet-maraging-steel-m300-for-200-w-powder-for-additive-manufacturing--96325?userLanguage=en&srsltid=AfmBOoq3HAz4jS0jcXDJMppmcNjfWZyIduCVDA8sYjGEslKZRXPXXTtO (accessed on 23 January 2025).
30. Davis, J.R.; ASM International (Eds.) *Carbon and Alloy Steels*; ASM Speciality Handbook; ASM International: Materials Park, OH, USA, 1996; ISBN 9780871705570.
31. *ASM International ASM Engineered Materials Reference Book*; ASM International: Metals Park, OH, USA, 1989; ISBN 9780871703507.
32. Carpenter. PowderRange M300 Data Sheet. Available online: https://www.carpenteradditive.com/hubfs/Resources/datasheets%202023/PowderRange_M300_Datasheet.pdf (accessed on 21 February 2025).
33. *ASTM B962-23*; Standard Test Methods for Density of Compacted or Sintered Powder Metallurgy (PM) Products Using Archimedes' Principle. American Society for Testing and Materials (ASTM): West Conshohocken, PA, USA, 2023.
34. Metalweb. Titanium Ti-6Al-4V (Grade 5), STA. Available online: https://www.matweb.com/search/datasheet.aspx?MatGUID=b350a789eda946c6b86a3e4d3c577b39&ckck=1 (accessed on 25 February 2025).
35. *International Standard ISO 8688*; Tool-Life Testing in Milling. ISO: Geneva, Switzerland, 1989.
36. Liang, X.; Liu, Z.; Wang, B.; Hou, X. Modeling of Plastic Deformation Induced by Thermo-Mechanical Stresses Considering Tool Flank Wear in High-Speed Machining Ti-6Al-4V. *Int. J. Mech. Sci.* **2018**, *140*, 1–12. [CrossRef]
37. Yue, C.; Li, X.; Liu, X.; Du, J.; Liang, S.Y.; Wang, L.; Sun, Y. Wear Behavior of Tool Flank in the Side Milling of Ti6Al4V: An Analytical Model and Experimental Validation. *Proc. Inst. Mech. Eng. Part C J. Mech. Eng. Sci.* **2022**, *236*, 1631–1644. [CrossRef]
38. Dynamic Metals. AMS 6411 Alloy Steel Data. Available online: https://dynamicmetalsltd.com/products/alloy-steel/4330-alloy-steel/ (accessed on 13 March 2025).
39. Dang, J.; Zang, H.; An, Q.; Ming, W.; Chen, M. Feasibility Study of Creep Feed Grinding of 300M Steel with Zirconium Corundum Wheel. *Chin. J. Aeronaut.* **2022**, *35*, 565–578. [CrossRef]